SCIENTIFIC REPORTS

OPEN

SUBJECT AREAS:
MATERIALS SCIENCE
NANOSCIENCE AND TECHNOLOGY

Received
6 August 2014

Accepted
4 November 2014

Published
26 November 2014

Correspondence and requests for materials should be addressed to H.O. (h.oyanagi@aist.go.jp)

§ Current address: Department of Material Sciences, Faculty of Engineering Sciences, Kyushu University, 6-1 Kasuga-Park, Fukuoka 816-8580, Japan.

* Current address: National Synchrotron Radiation Laboratory, University of Science and Technology of China, Hefei, Anhui 230029, PR China.

† Current address: Division of Functional Materials and Nano Devices, Ningbo Institute of Material Technology & Engineering, Chinese Academy Sciences, Ningbo 315201, PR China.

‡ Current address: Advanced Intellectual Property Research Institute, Co., Ltd., 4-4-10 Shiba, Minato-ku, Tokyo 108-0014, Japan.

Nanoclusters Synthesized by Synchrotron Radiolysis in Concert with Wet Chemistry

Hiroyuki Oyanagi[1], Yuuichi Orimoto[2]§, Kuniko Hayakawa[3], Keisuke Hatada[3,4], Zhihu Sun[1]*, Ling Zhang[5]†, Kenichi Yamashita[2], Hiroyuki Nakamura[2], Masato Uehara[2], Atsuyuki Fukano[1]‡ & Hideaki Maeda[2,5,6]

[1]Photonics Research Institute, National Institute of Advanced Industrial Science and Technology (AIST), 1-1-1 Umezono, Tsukuba, Ibaraki 305-8568, Japan, [2]Measurement Solution Research Center, National Institute of Advanced Industrial Science and Technology, 807-1 Shuku-machi, Tosu, Saga 841-0052, Japan, [3]INFN Laboratori Nazionali di Frascati, c.p. 13, I-00044 Frascati, Italy, [4]Groupe Théorie, Département Matériaux-Nanosciences, Institut de Physique de Rennes, UMR CNRS-UR1 6251, Université de Rennes-1, 35042 Rennes cedex, France, [5]Department of Molecular and Material Sciences, Interdisciplinary Graduate School of Engineering Sciences, Kyushu University, 6-1 Kasuga-koen, Kasuga, Fukuoka 816-8580, Japan, [6]CREST, Japan Science and Technology Agency, 4-1-8 Hon-chou, Kawaguchi, Saitama 332-0012, Japan.

Wet chemical reduction of metal ions, a common strategy for synthesizing metal nanoparticles, strongly depends on the electric potential of the metal, and its applications to late transition metal clusters have been limited to special cases. Here, we describe copper nanoclusters grown by synchrotron radiolysis in concert with wet chemistry. The local structure of copper aggregates grown by reducing Cu(II) pentanedionate using synchrotron x-ray beam was studied *in situ* by x-ray absorption spectroscopy. A detailed analysis of the XANES and EXAFS spectra, compared with DFT calculations and full-potential non-muffin-tin multiple scattering calculations, identified the nanocluster as Cu_{13} with icosahedral symmetry. The novel "charged" nanoclusters tightly bound to electron-donating amido molecules, which formed as a result of photo-induced deprotonation of ligand amines, were stabilized by irradiation. Monodispersive deposition of nanoclusters was enabled by controlling the type and density of "monomers", in remarkable contrast to the conventional growth of metallic nanoparticles.

Metal nanoclusters (NCs) have attracted great interest in fundamental science and industrial applications over the past decade, because of size-dependent properties such as tailoring of optical gap[1], unusual magnetism[2], or enhanced catalytic activity[3]. Ligated (wet) NCs are of particular interest to researchers anticipating novel catalytic functions through strong perturbations of the electron states of the cluster core by ligand molecules.

Late transition metal NCs are obtained by stabilizing against aggregation into larger nanoparticles (NPs). In contrast to noble metal clusters, such as gold NCs synthesized by agglomeration from colloidal solution[4,5], late transition metal clusters are typically difficult to stabilize because of an intrinsic stability as ions arising from an atom-specific electron configuration[6]. Despite advances in wet synthesis methods, *e.g.*, two-phase synthesis[5] and real-time monitoring of reactions by *in situ* local probes[7,8], stabilizing smaller NCs has long been a challenge to researchers[9,10].

The principle of wet chemistry synthesis of late transition metal NCs involves a simple reduction of multivalent ions, which is strongly dependent on the standard electrode potential (SEP). Taking copper as an example, which contrasts with a more positive SEP metal such as gold, most previous studies focused on special cases with a stabilization mechanism such as weakly interacting environments (*e.g.*, solid argon)[11,12] or strongly interacting ligation. In fact, in our previous work on Cu_{13} NCs prepared by wet chemistry in a microfluidic cell[13], rapid reduction, particularly at elevated temperature, led to an immediate nucleation of monomers and subsequent growth. According to classical nucleation theory (CNT)[14], nucleation is the localized appearance of a new phase (monomers) from a supersaturated phase and the density of monomers must be minimized to decrease the probability of forming multimers (nucleus). Thus, we anticipated that if the precursor stabilizes multivalent ions against reduction, the reduction kinetics would slow down and decrease the density of monomers.

On the other hand, it has been recognized that radiation-induced reduction (radiolysis) of aqueous solutions form monodispersed metallic NPs[15,16] or NCs[17]. The advantage of radiolysis[18] using synchrotron radiation is its atomic tunability and controllability of doses (irradiation parameters such as photon energy, band path, flux, polarization, and elapsed time, *etc.*). By tuning the photon energy to the core level of atoms of interest, one can selectively create core holes, ionize atoms, excite electrons to unoccupied anti-bonding states, thus causing bond breaking and generating secondary electrons. Although bond energies (*e.g.*, for the N-H bond, $D_0 = \Delta H \approx$ 385 kJ/mol) lie in the VUV to soft x-ray regime (<600 eV), secondary electrons are a common feature of the radiation effect with higher energy (hard x-ray) excitation. Interestingly, the effect of secondary electrons ejected to the vicinity of excited atoms may provide a novel means of selective (local) reduction. In this paper, we describe how synchrotron radiolysis combined with wet chemistry can stabilize late transition metal NCs, choosing copper as a model system. The results point to a novel category of nanomaterial-charged NCs.

Results

Nanoclusters formed by synchrotron radiolysis. In our previous study on Cu NCs, the reaction process consisted of the two sequential procedures illustrated in Fig. 1(a): ligation to form a divalent planar amino-complex (R1) and a subsequent reduction procedure (R2)[13]. The reduction of Cu^{2+} to Cu^0 is, in general, a two-step reaction: the first reduction to Cu^+ ions and the second "disproportionation" into Cu^{2+} ions and Cu^0 monomers (R3: $2Cu^+ \rightarrow Cu^{2+} + Cu^0$), which reflects the stability of Cu^{2+} ($3d^9$) states over Cu^+ ($3d^{10}$) states, because of the strong metal-ligand interaction. As the stability of ions depends on ionization potential as well as solvation energy, we conducted extensive screening experiments to find the optimum reaction conditions (combinations with various chemical substances and concentrations), trying to shift $R2_{eq}$ toward Cu^{2+} ions (or suppressing Cu^+ ions) to slow down R3 kinetics. Suppression of the bottleneck reaction (R3) was anticipated to lower the density of metal monomers, which is proportional to the nucleation rate, and therefore the nucleus density.

The equilibrium precursor solution ($R2_{eq}$) was prepared from four-fold planar Cu(II) complexes, as described in TABLE I, in an inert (N_2) atmosphere at room temperature. The precursor solution (total volume of 1.5 ml) was prepared for C1 and S, with a constant concentration of Cu^{2+} ions (2.4 mM/l). Extreme care was taken to avoid air exposure so that oxidation would not occur by performing all reactions in a vacuum-tight glovebox. The equilibrium solution filled into a TEFLON cell with a KAPTON window was irradiated for 4 h with a focused undulator x-ray beam (1×10^{12} photons/s) at 9.0 keV using the NW2A of the 6.5 GeV PF-AR at High Energy Accelerator Research Organization, Tsukuba. During the *in situ* XAS experiments, we found that synchrotron radiolysis of $R2_{eq}$, tuned to the Cu K-shell excitation, changed the copper valence of the precursor solution and copper aggregates were simultaneously formed on the x-ray window. The nature (growth mode and particle size) of aggregates strictly depended on the $R2_{eq}$ which was measured by K ($K = [Cu^{2+}]/[Cu^+]$). See Fig. S1 in Supporting Materials for the experimental determination of K-values. We focused on the two extreme cases: the Cu^+-dominant $R2_{eq}$ ($K = 0$), which led to a control denoted as C1, and Cu^{2+}-dominant $R2_{eq}$ ($K = 3.2$), which deposited a cluster sample S. The photo-induced reduction of the precursor solution and aggregation were monitored by *in situ* XAS (Fig. S5, Supporting Materials) and a telescopic TV camera (Fig. 1(a)). The *in situ* XAS measurement of the aggregates (C1 and S) separated from the precursor solution showed that a very thin and flat layer of small clusters is deposited when $K \gg 1$ by synchrotron radiolysis on a nitrogen-terminated organic film (KAPTON), as shown in Fig. 2(c).

It is well known that irradiation of organic solutions causes electronic excitation and bond-breaking, generating radicals, *e.g.*, negatively charged alkyl ions, and H^+. Although the effect of irradiation can in general be complicated, the effect of monochromatic x-ray irradiation here can safely be described as a donation of secondary

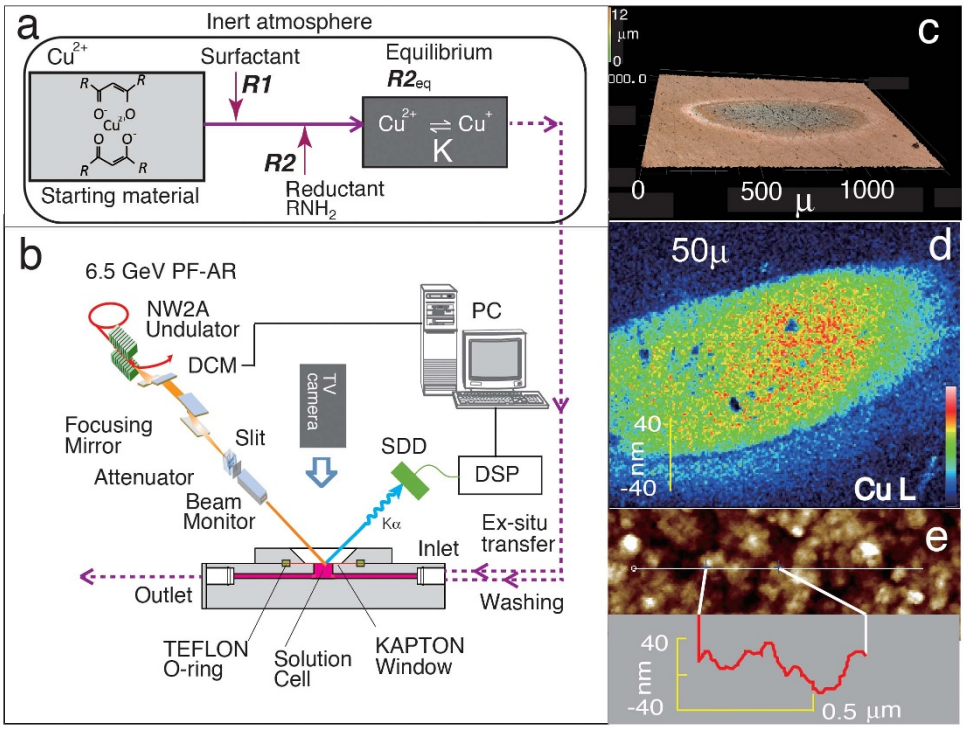

Figure 1 | Schematic of experimental setup; *ex situ* reaction for preparing the precursor equilibrium solution, $R2_{eq}$ (a). Synchrotron radiolysis and the subsequent *in situ* x-ray absorption spectroscopy (b). Interference microscopy (c) and Cu L x-ray 2D images (d) of S. AFM 3D image and linear profile for S (e).

Table I | Chemical substances, concentrations and reaction time used for preparing the equilibrium solution $R2_{eq}$

Specimen (Valency at equilibrium)	Starting Material	Reductant	Surfactant	Solvent	Reaction time
Control, C1 (1)	Cu(II) bis(1,1,1,5,5,5-hexafluoro-2,4-pentanedionate), $Cu(II)[HFPD]_2$,	benzopinacol $C_{26}H_{22}O_2$ (BP)	Octylamine $C_8H_{19}N$ (OCA)	diethylene glycol diethyl ether $C_8H_{18}O_3$ (DGDE)	1 h
Concentration	2.4 mM/L	48 mM/L	48 mM/L		
Sample, S (1.76)	Cu(II) bis(2,2,6,6-tetramethyl-3,5-heptanedionate), $Cu(II)[TMHD]_2$,	trimethylamine borane $C_3H_{12}BN$ (TMAB)	oleylamine $C_{18}H_{37}N$ (OLA)	diethylene glycol diethyl ether $C_8H_{18}O_3$ (DGDE)	120 h
Concentration	2.4 mM/L	4.8 mM/L	28.8 mM/L		

The equilibrium solution was irradiated by a 9.0-keV x-ray beam with a flux of 1×10^{12} photons/s for 4 h.

electrons or a photo-reduction in the vicinity of absorbed atoms. Thus, in the $K = 0$ case (C1), the Cu^+ intermediates were reduced to Cu^0 monomers and likewise the Cu^{2+} planar complexes were reduced mostly to Cu^+ monomers in the $K \gg 1$ case (S). As seen in Figs. 1(c) and (d), the 2D mapping optical and x-ray images for S reveal that copper aggregates were formed on the focused x-ray beam spot (600 $\mu m^{(H)} \times 300\ \mu m^{(V)}$), which was horizontally expanded for geometrical reasons (an incidence angle of 45°). The AFM data for S in Fig. 1(e) indicate a smooth surface (surface roughness ≈ 80 nm) resulting from a very slow deposition rate (~10 nm/h).

XAS experiments and analysis. In Fig. 2(a), the Cu K-XANES spectra for $R2_{eq}$ (C1), measured as an average of the reactant solution and aggregates, show the evolution of the near-edge features upon irradiation, indicating a gradual change from the Cu^{2+} to Cu^0 states, linear with respect to elapsed time. Such photo-reduction of copper ions was also found at other synchrotron radiation beamlines that provide high-flux photon beams, typically 10^{12} photons/s[19]. Characteristic features A–D in the XANES data for $R2_{eq}$ after irradiation match with well-known signatures of fcc metals. By contrast, for separated aggregates recovered by *in situ* washing of the solution cell (Fig. 1(b)), the irradiation effect gave remarkably different XANES spectra. Strikingly, the results indicated that the radiolysis product depends on $R2_{eq}$ (the *K*-value); Figs. 2(b) and (c) show that the irradiation-induced aggregates C1 and S are fcc-like NPs and NCs, respectively. In contrast to the control, S exhibited featureless near-edge structures indicative of a small cluster ($n < 19$)[13].

The Cu^+ state is often associated with a sharp 1*s*-4*p* transition due to a "shakedown" process simultaneously with a ligand-to-metal charge transfer[20], which is strongly polarized in the axial ligand direction. The inset blowup of the 1*s*-4*p* transition shows that the peak shifts slightly to higher energies in the case of S relative to the completely metallic energy level for C1, pointing to a possible incomplete

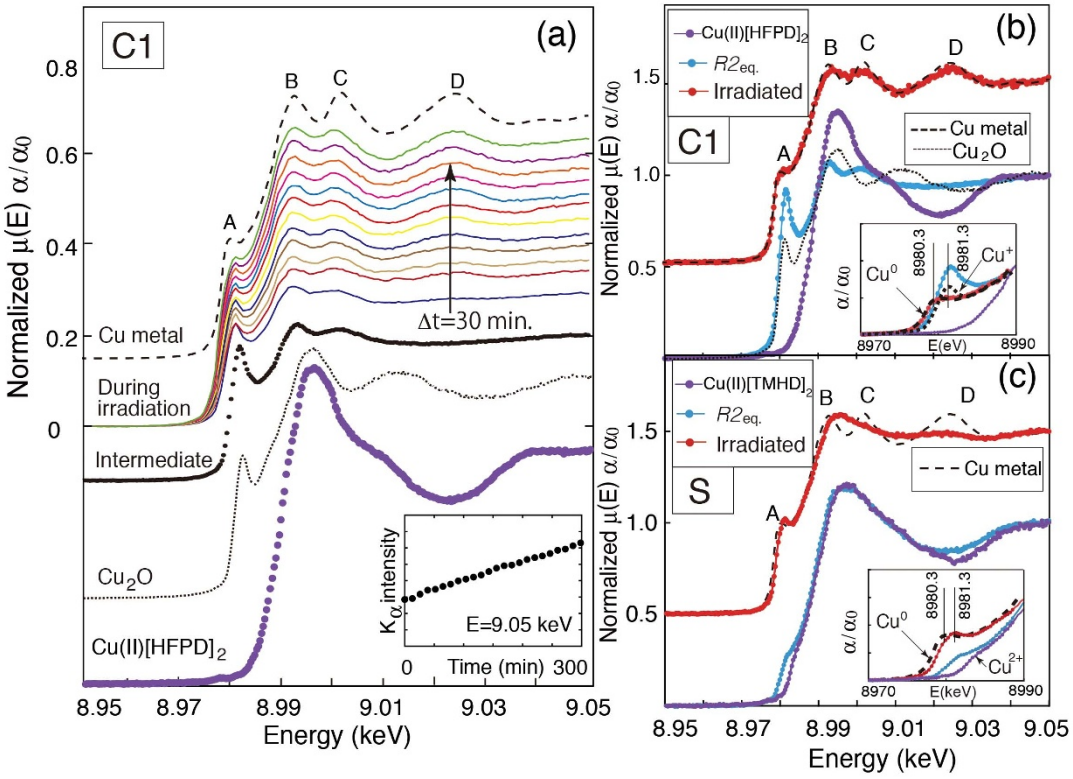

Figure 2 | Evolution of Cu K-XANES spectra for $R2_{eq}$ during irradiation, together with those for the references $Cu(II)[HFPD]_2$, Cu_2O and Cu metal. The inset plots the intensity variation of the fluorescence signal at 9.05 keV during irradiation for C1 (a). Cu K-XANES spectra for C1 and $R2_{eq}$ before irradiation and the references, *viz.*, an fcc metal, Cu_2O, and $Cu(II)[HFPD]_2$. The inset is a blowup of the 1*s*-4*p* transition (b). Cu-K XANES spectra for S compared with those of $R2_{eq}$ before irradiation and of the references, *viz.*, an fcc metal and $Cu(II)[TMHD]_2$ (c).

photo-reduction that left some copper atoms positively charged after clustering. The intermediate energy position of the 1*s*-4*p* transition, which is absent for NPs[12], could be common to small clusters with a large optical (HOMO-LUMO) gap unlike fcc metals or NPs[11–13]. The 1*s*-4*p* transition for S lies close to that of the Cu^+ state, indicative of an intermediate valence state, although the true electron configuration of copper atoms in NCs (S) remains an open question.

In Fig. 3(a), normalized EXAFS oscillations multiplied by k^2 are plotted as a function of photoelectron wavenumber, *k*, for C1, S, and an fcc metal (reference). It can be seen that although the EXAFS oscillations for C1 resemble those of an fcc lattice, those for S are significantly different both in magnitude and profile. The low-*k* region indicated by an arrow at $k = 3$ Å^{-1} (inset) shows a systematic increase in magnitude, evidence for the emergence of a low-*z* element (nitrogen) in the nearest neighbor (N.N.) shell with decreasing size.

In the Fourier transform of the k^2-weighted $\chi(k)$ functions (Figs. 3(b) and (c)), a prominent N.N. peak at $R = 2.2$ Å decreases sharply in magnitude for C1 and, more significantly, for S. The magnitude drop in the N.N. peak is caused by a size variation[21], as well as increased defects and disorder. The FT magnitude for S shows a strikingly different double peak consisting of (short) Cu-N bonds and (long) Cu-Cu bonds, which is evidence for a small cluster, consistent with the emergence of a low-*z* element scatterer (Fig. 3(a)). The emergence of Cu-N bonds is indicative of a ligated small cluster, which contains information on the cluster size and ligand coordination.

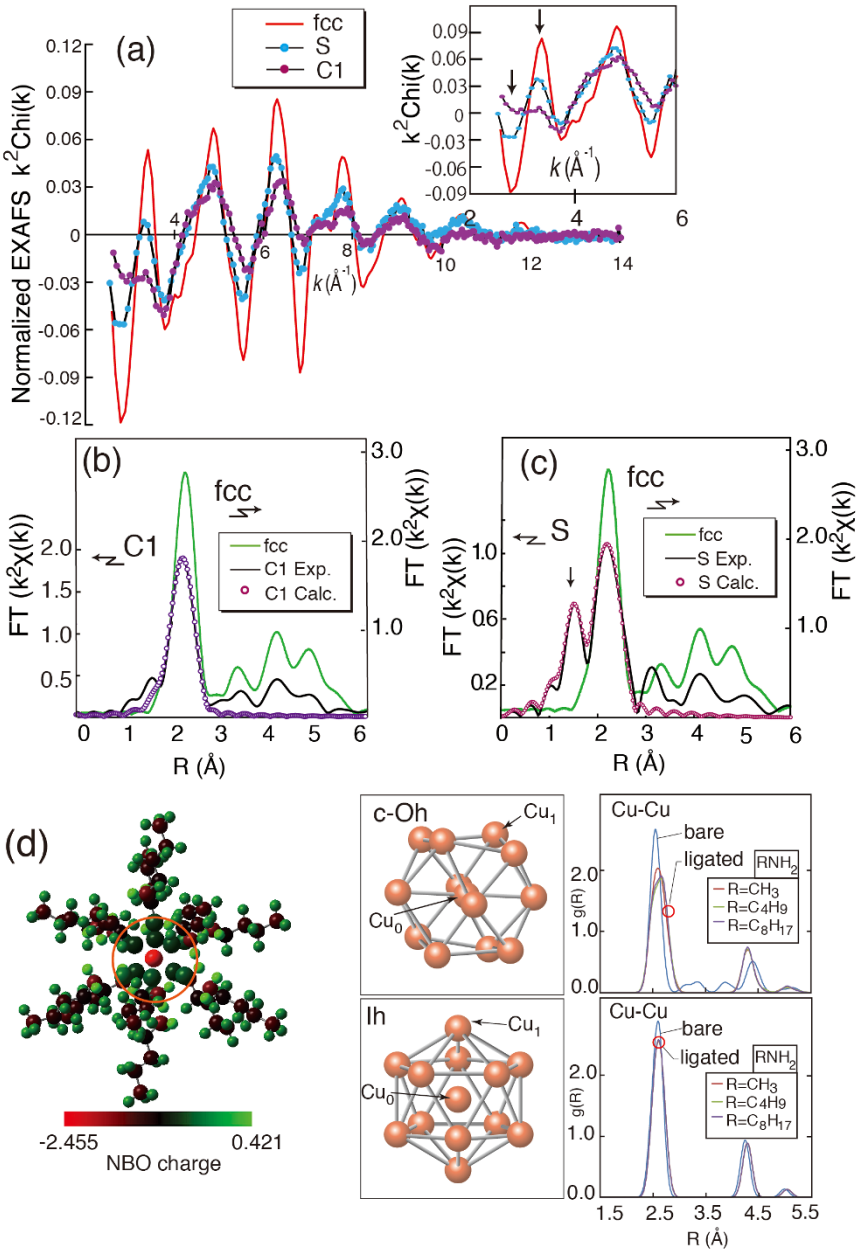

Figure 3 | EXAFS oscillations as a function of wavenumber, *k*, for C1 and S, compared with those of an fcc metal (a). The inset shows a blowup of the low-*k* region ($k = 2.5$–6 Å^{-1}). The Fourier transform magnitude functions for C1 (b) and S (c). Open circles denote the curve-fitted results compared to the reference (an fcc metal). Model structure for the Cu_{13} ligated with various amines, derived by DFT geometrical optimization. Inhomogeneous electron distribution (NBO net charge) is displayed in a graded color scale. Local structures for Cu_{13} clusters with *Ih* and *c-Oh* symmetry and RDFs shown in separate columns (d).

Table II | Results of the curve fit analysis of the EXAFS oscillations

Sample	Bond	*N*	*R* (Å)	σ^2 (10^{-3} Å^2)	ΔE_0 (eV)
C1	Cu-Cu	7.3 ± 1.4	2.56 ± 0.04	9.8 ± 1.7	2.3
S	Cu-N	0.7 ± 0.3	1.90 ± 0.02	3.2 ± 2.0	4.6
	Cu-Cu	3.5 ± 0.6	2.56 ± 0.05	7.6 ± 1.6	1.3

For C1 and C2, a single-shell model was fit to the experimental EXAFS oscillations times k^2 in *k*-space. For S, a two-shell model was used to account for the Cu-Cu and Cu-N contributions.

The open circles in the FT magnitude in Figs. 3(b) and (c) show the results of curve fitting in *k*-space (Table II). The size-dependent magnitude variation in the N.N. peak is consistent with previous studies[21], while a similar short M-L bond was reported in the case of noble metal clusters[8]. The average coordination numbers of the Cu-N and Cu-Cu bonds, 0.7 ± 0.3 and 3.5 ± 0.6, respectively, were consistent with our DFT optimization of model clusters consisting of thirteen atoms. Montano *et al.*[11] and Tamura *et al.* reported much shorter Cu-Cu distances in solid Cu NCs[22] prepared onto solid argon and a *p*-type GaAs (100) surface, respectively. In our experiment, the observed Cu-Cu distance, 2.56 Å (S), was close to the fully relaxed bond[23]. The disorder parameter, σ^2, fell in the range of 7.6–9.8 (10^{-3} Å^2), in good agreement with Jayanetti *et al.*[19]. Compared to the Cu-N distance in Cu^{2+} complexes such as 2.05 Å $[Cu(H_2O)_2(NH_3)_4]$ or 2.08 Å in the pyridine complex, the short Cu-N distance (1.90 Å) remains puzzling. Such a short distance implies a strong interaction between the surface atoms and ligand molecules which may provide a clue to interpreting the 1*s*-4*p* peak shift.

Discussion

NCs prepared by radiolysis consist of a small number of atoms (n = 13–19). Taking into account the coordination number evaluated by EXAFS analysis, we chose a model cluster of thirteen atoms[12,13]. Let us first focus on the possible model clusters with different symmetries, *viz.*, icosahedron (*Ih*), cubo-octahedron (*c-Oh*), hexagonal close-packed (*hcp*), bicapped double-decker sandwich, *etc.*[24]. First-principle calculations on bare clusters ($n \leq 10$)[25,26] have established the structural evolution of electron affinity and ionization potential, reflecting the electronic shell and subshell closing. One of the most striking results was the inhomogeneous electron distribution illustrated in the map of NBO charge (net charge) in Fig. 3(d). Using the optimized atomic coordinates of the ligated model cluster,

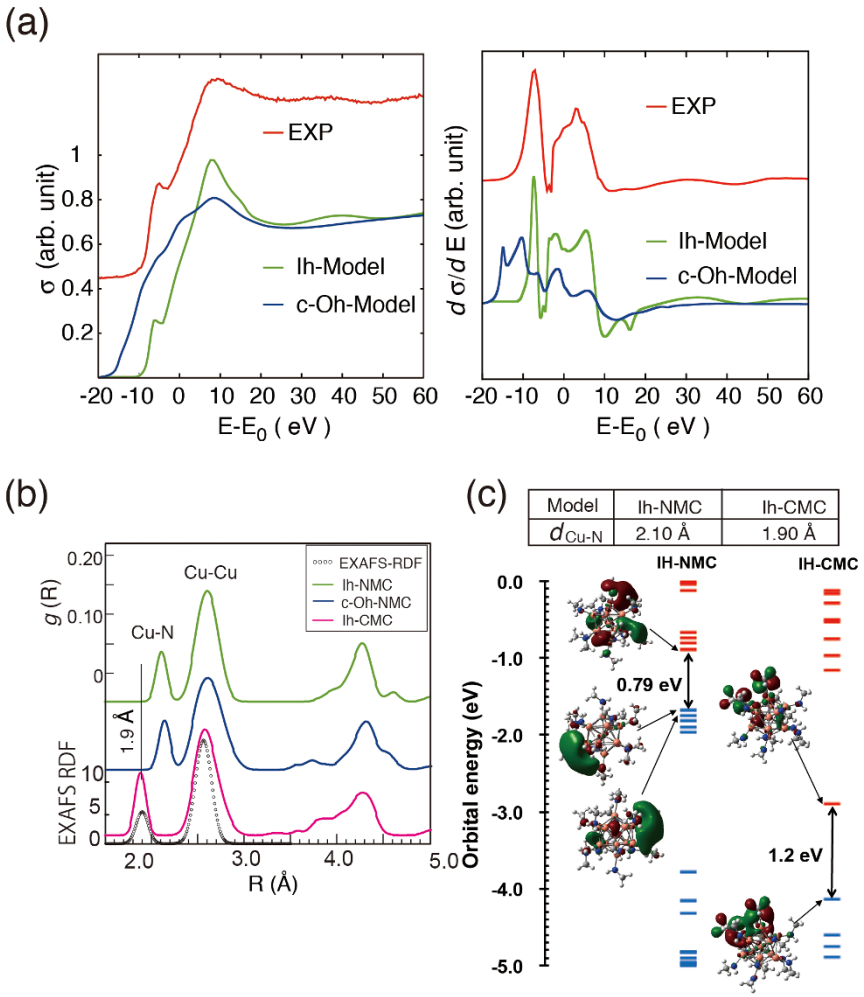

Figure 4 | Theoretical Cu K-XANES spectra for Cu_{13} clusters with *Ih* and *c-Oh* symmetry, obtained by the FPMS calculation, compared with the experiment (a). The RDFs calculated for the *Ih* and *c-Oh* model clusters coordinated with ligand amine RNH_2 (neutral model cluster, NMC) and deprotonated amido RNH^- (charged model cluster, CMC) (b). Orbital energy diagram (α-spin orbitals only, for simplicity) with the HOMO-LUMO gap also illustrated (c).

XANES spectra were calculated by the full potential multiple scattering (FPMS) approach beyond the muffin-tin approximation[27]. For localized systems such as NCs, the muffin-tin approximation often fails and FPMS is required[27]. The XANES spectra were calculated on the basis of geometrically optimized atomic coordinates for ligated model clusters using the FPMS approach.

Our DFT calculation of all possible symmetry cases narrowed down the candidates to the two symmetry models *Ih* and *c-Oh*. A comparison of the experimental XANES for S with the FPMS calculation (Fig. 4(a)) indicates that the symmetry is likely to be icosahedral, consistent with recent work on Cu clusters in Ar shells[12]. Our analysis of the radial distribution functions (RDFs) revealed that the structural difference between the *Ih* and *c-Oh* models is essentially the broader distribution of the second shell in the *Ih* symmetry. This rearrangement of the second shell could minimize the Cu-Cu distance variation and lower the Coulombic repulsion between surface atoms. Also, the absence of the experimental double-peak XANES feature around 9,000 eV observed for $n > 43$ (an fcc lattice) in Fig. 2(c)[12,13] is consistent with the symmetry of the model cluster. Highly distorted nature of the *Ih* cluster was reported by computational studies for bare Cu_{13} and Au_{13}[29] while for $M@Au_{12}$ series of clusters (M = W, Mo), the *Ih* symmetry is lower in energy than the *Oh*[30]. As the symmetry dependence of stability for the two cases is marginal, it is likely that the metal-ligand interaction becomes crucial.

The RDFs in Fig. 4(b) calculated for optimized model structures were compared with the EXAFS-RDF constructed from the experimental structural parameters of EXAFS analysis (Table II). The N.N. region was well reproduced by the optimized "neutral" model cluster (NMC) consisting of 13 Cu^0 atoms. However, the metal-ligand interaction in this model cluster appears to be underestimated, as the experimental Cu-N distance (1.90 Å) is 0.2 Å shorter than that in the model.

Thus, we examined a "charged" model cluster ("CMC") in Fig. 4(b), in contrast to NMC ("*Ih*-NMC" and "*c-Oh*-NMC" in the same panel). The CMC is highlighted by twelve positively charged surface atoms ligated with highly electron-donating molecules canceling the local charge imbalance. Amido (RNH^-), which is formed by radiation-induced deprotonation, is more likely to serve as an electron donor than amine (RNH_2). N−H bond-forming and -breaking processes often relate to catalytic activities such as ammonia synthesis[31] and occur by photon irradiation. Recent work by Jonson *et al.*[32] suggested that decay processes, rather than photoexcitation, generate a large number of secondary electrons, which would populate the antibonding orbitals and thus initiate bond-breaking. As a result, an amido complex with low-valence metal ions would strengthen the M-L bond and be detectable as a bond length shortening. Indeed, the RDF calculated for CMC gave a Cu-N distance (1.90 Å) in good agreement with the experimental value.

The calculated HOMO-LUMO gaps ligated by methyl amine were 0.79 and 0.73 eV for *Ih*-NMC and *c-Oh*-NMC, respectively, in remarkable contrast to the 1.2 eV for *Ih*-CMC (Fig. 4(c)). The large HOMO-LUMO gap of CMC is consistent with the observed short Cu-N distance. The MO levels and their shapes around the gap in Fig. 4(c) and Fig. S5, where only α-spin orbitals are shown for simplicity, suggest that the electronic states of the two models are quite different. Compared with congested MOs in NMC, discrete MOs with different shapes are found around the gap in CMC. The frontier MOs from HOMO-4 to LUMO+3 in NMC consist of σ-type orbitals over the space extending to the ligands or surface Cu atoms. In contrast, the HOMO and LUMO in CMC are due to π-type orbitals localized to the Cu-N-C bonds. The difference on the frontier MOs may lead to a different redox reactivity.

How does the precursor equilibrium $R2_{eq}$ between Cu^{2+} ions and Cu^+ ions control the product of synchrotron radiolysis? In the case of C1, with its strong reducing power (see Table I), wet chemistry (R2)

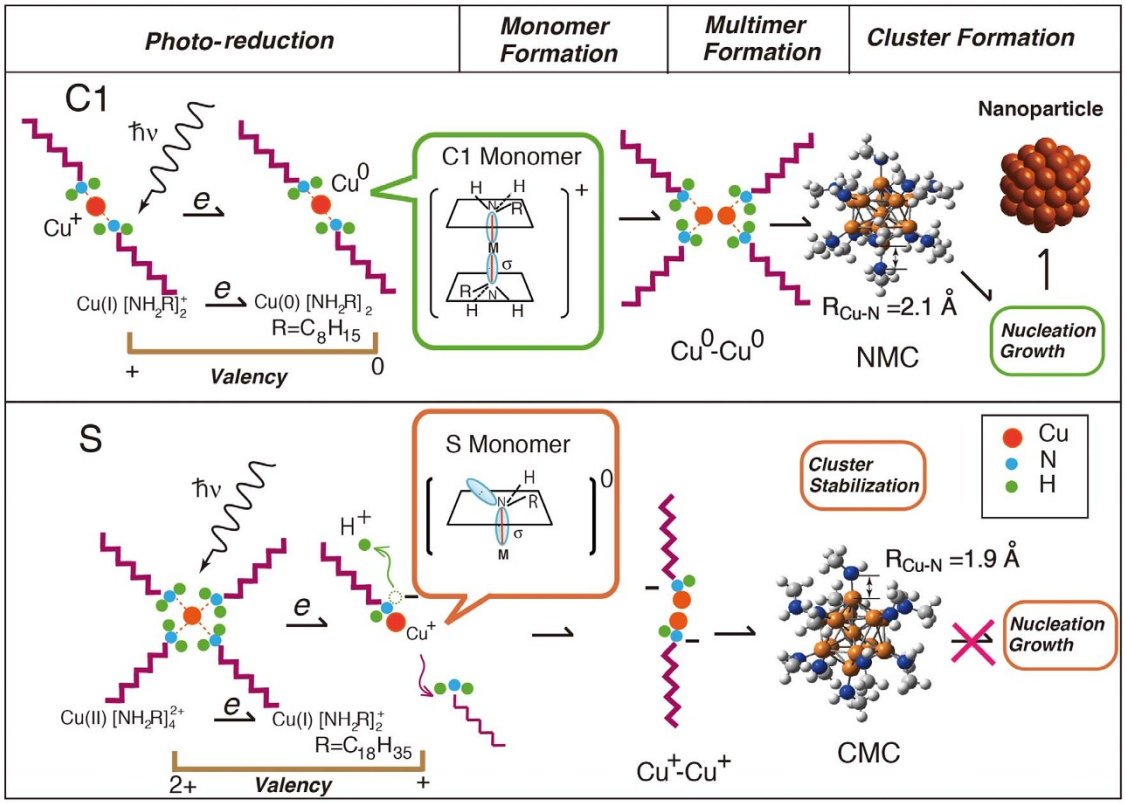

Figure 5 | Schematic representation of the formation mechanism of Cu CMC (S) in comparison with that of NMC (C1) by radiolysis, which leads to different monomer types and densities depending on the precursor equilibrium, $R2_{eq}$.

completely transforms Cu^{2+} ions into Cu^{+} ions (See Fig. 2(c)). The disproportionation reaction (R3) converts half of the Cu^{+} ions into Cu^{0} monomers ligated by amine molecules. In contrast, the $R2_{eq}$ for S is dominated by the Cu^{2+} states, owing to an extremely slow kinetics or a strong reverse reaction, which would lead to monomer starvation.

In our schematic model (Fig. 5), what determines the nature of radiolysis is the type and density of "monomers". The pathway to CMC is governed by its monomer ligated to amido whose σ orbital strongly interacts with the Cu^{+} 4s and 3d orbitals, which would be further strengthened by π orbital overlapping as a result of hybridization change from sp^3 nitrogen atom (tetrahedral) to sp^2 one (trigonal planar) upon the formation of CMC, in sharp contrast to a linear complex with two ligand amines with sp^2 nitrogen atom in the case of NMC. For $K = 0$, photo-reduction eventually creates Cu^{0} monomers (amine complexes) that assemble into nuclei, which later grow into NPs. In contrast, for $K \gg 1$, the monomer is a singly ligated amido whose nitrogen atoms are strongly bound to surface copper atoms (Fig. 5). Such Cu^{+} amido complexes may also exist in the case of C1, but they would be overwhelmed in density by the Cu^{0} monomers.

In this work, wet chemistry and radiolysis controlled the type and density of "monomers" in a concerted fashion, so that nucleation is suppressed while charged clusters are stabilized. We show that combining the advantages of these two complementary reducing techniques could provide a novel means of stabilizing late transition metal clusters with unique electronic states.

Methods

X-ray absorption spectroscopy. XAS spectra were measured in the fluorescence mode with an energy resolution of ~1.5 eV (9 keV). The EXAFS oscillation functions were extracted using ATHENA[33], and least-squares parameter fitting was performed using ARTEMIS[33], both of which were implemented in the IFEFFIT package[34]. The k^2-weighted $\chi(k)$ functions were Fourier transformed into R-space using a Hanning window over a typical k-range of 2.5–10.5 $Å^{-1}$. The *ab initio* multiple-scattering code FEFF8.20 with the muffin-tin approximation and FPMS[27] and MXAN[35] codes for the full potential multiple scattering calculation were used for the calculation of XANES for model clusters.

DFT calculations. The DFT calculations were performed to obtain the optimized geometries and electronic structures of model clusters. These NCs were treated as open-shell systems and calculated by the unrestricted scheme of Becke's three-parameter hybrid functional with the correlation functional of Lee, Yang, and Parr, *i.e.*, uB3LYP[36]. The LanL2DZ basis set was adopted for all DFT calculations. In the LanL2DZ, the double-zeta functions and Los Alamos effective core potential (ECP) were adopted for valence and core electrons of the Cu atom, respectively[37]. On the other hand, the Dunning/Huzinaga valence double-zeta functions (D95V)[38] were adopted for the other atoms (H, C, and N) in the basis set. For the DFT calculations, out of possible model symmetries, four models with different symmetries were taken into account, *i.e.*, icosahedron (*Ih*), cubo-octahedron (*c-Oh*) or face-centered cubic (fcc), hexagonal close-packed (*hcp*) or truncated hexagonal bipyramid and bicapped double-decker sandwich of five-fold geometry (bicapped)[24]. Although those models optimized as a bare cluster in vacuum at $T = 0$ K do not always give the lowest energy structure under the realistic condition[39], those models can be candidates for liganded clusters in solution at a finite temperature.

Four different model structures were prepared by GaussView 5.0 and the geometrical parameters were fully optimized without symmetry constraints by the Gaussian09 program package. The lowest energy spin multiplicities were studied for a neutral bare cluster over seven different spin multiplicities 2, 4, 6, 8, 10, 12 and 14. Out of starting four different symmetries, most stable spin multiplicity was found for the two models *Ih* and *c-Oh*, with spin multiplicity $S = 6$ and 2, respectively while other two models (hcp and bicapped) failed to keep the symmetry during the optimization. The energy minima were confirmed for the *Ih* and *c-Oh* models by performing a frequency analysis.

On the other hand, for amine liganded clusters, there are numerous possibilities on the conformation of 12 amine molecules. It is very hard to determine the lowest energy spin multiplicities for the liganded cluster because a lot of local minimum structures are expected. Therefore, for simplicity, the ground-state spin multiplicities $S = 6$ and 2 determined for the bare Cu_{13} nanoclusters were adopted for the amine liganded Cu_{13} models with *Ih* and *c-Oh* symmetries, respectively. Natural bond orbital (NBO) population analyses (Gaussian NBO Version 3.1) were applied to find out the charge distribution on the optimized structures, which were illustrated by GaussView 5.0.

1. Aiken III, J. D. & Finke, R. G. A review of modern transition-metal nanoclusters: their synthesis, characterization, and applications in catalysis. *J. of Mol. Catal. A: Chemical* **145**, 1–44 (1999).
2. Crespo, P. *et al.* Permanent Magnetism, Magnetic Anisotropy, and Hysterisis of Triol-Capped Gold Nanoparticles. *Phys. Rev. Lett.* **93**, 087204–087208 (2004).
3. Haruta, M. *et al.* Gold Catalysts Prepared by Coprecipitation for Low-Temperature Oxidation of Hydrogen and of Carbon Monoxide. *J. Catal.* **115**, 301–309 (1989).
4. Faraday, M. The Bakerian Lecture: Experimental Relations of Gold (and Other Metals) to Light. *Philos. Trans. R. Soc. London*, **147**, 145–181 (1857).
5. Brust, M. *et al.* Synthesis of Thiol-derivatised Gold Nanoparticles in a Two-phase Liquid-Liquid System. *J. Chem. Soc. Chem. Commun.*, Issue **7** 801–802 (1994).
6. Watzky, M. A. *et al.* A New Mechanism When Hydrogen Is the Reductant: Slow, Continuous Nucleation and Fast Autocatalytic Surface Growth. *J. Am. Chem. Soc.* **119**, 10382–10400 (1997).
7. Smolentsev, G. & Soldatov, A. V. Quantum local structure refinement from XANES: multi-dimensional interpretation approach. *J. Synch. Rad.* **13**, 19–29 (2006).
8. Yao, T. *et al.* Probing Nucleation Pathways for Morphological Manipulation of Platinum Nanocrystals. *J. Am. Chem. Soc.*, **134**, 9410–9416 (2012).
9. Ostwald, W. Stüdien uber die Bildung und Umwandlung fester Körper. *Zeitschrift für physikalische Chemie*, **22**, 289–330 (1897).
10. Nishijima, S. *et al. In Situ* Time-Resolved XAFS Study on the Formation Mechanism of Cu Nanoparticles Using Poly (N-vinyl-2-pyrrolidone) as a Capping Agent. *Langmuir* **26**, 4473–4479 (2010).
11. Montano, P. A. *et al.* Structure of Copper Monoclusters Isolated in Solid Argon. *Phys. Rev. Lett.* **56**, 2076–2079 (1986).
12. Mazalova, V. L. *et al.* Small Copper Clusters in Ar Shells: A Study of Local Structure. *J. Phys. Chem. C* **113**, 9086–9091 (2009).
13. Oyanagi, H. *et al.* Small copper clusters studied by x-ray absorption near-edge structure. *J. Appl. Phys.* **111**, 084315–084319 (2012).
14. LaMe, V. & Dinegar, R. H. Theory, Production and Mechanism of Formation of Monodispersive Hydrosols. *J. Am. Chem. Soc.* **72**, 4847–4854 (1950).
15. Buxton, G. V. & Green, J. C. Reactions of some simple α- and β-hydroxyalkyl radicals with Cu^{2+} and Cu^{+} ions in aqueous solution. A radiation chemical study. *J. Chem. Soc. Faraday Trans.* I **74**, 697–714 (1978).
16. Freiberg, M. & Meyerstein, D. Reactions of aliphatic free radicals with copper cations in aqueous solution Part 2.-Reactions with cupric ions: a pulse radiolysis study. *ibid* **76**, 1825–1837 (1980).
17. Khatouri, J. *et al.* Radiation-induced copper aggregates and oligomers. *Chem. Phys. Lett.* **191**, 351–356 (1992).
18. Jonah, C. D. A short history of the radiation chemistry of water. *Radiat. Res.* **144**, 141–147 (1995).
19. Jayanetti, S. *et al.* Analysis of radiation-induced small Cu particle cluster formation in aqueous $CuCl_2$. *J. Chem. Phys.* **115**, 954–962 (2001).
20. Bair, R. A. & Goddard, W. A. *Ab initio* studies of the x-ray absorption edge in copper complexes I. Atomic Cu^{2+} and $Cu(II)Cl_2$. *Phys. Rev.* B **22**, 2767–2776 (1980).
21. Roscioni, O. M. *et al.* Computational prediction of L_3 EXAFS spectra of gold nanoparticles from classical molecular dynamics simulations. *Phys. Rev. B* **83**, 115409–115417 (2011).
22. Tamura, K. *et al.* Structural Study of Electrochemically Deposited Cu on p-GaAs(100) in H_2SO_4 Solution by In Situ Surface-Sensitive X-ray Absorption Fine Structure Measurements. *J. Phys. Chem.* B **104**, 9017–9024 (2000).
23. Mesu, J. G. *et al.* Probing the Influence of X-rays on Aqueous Copper Solutions Using Time-Resolved in Situ Combined Video/X-ray Absorption Near-Edge/Ultraviolet-Visible Spectroscopy. *J. Phys. Chem.* B **110**, 17671–17677 (2006).
24. Demuynck, J. *et al.* Bulk properties or not: The electronic structure of small metal clusters. *ibid.*, **75**, 3443–3453 (1981).
25. Massobrio, C. *et al.* Structural and electronic properties of small Cu_n clusters using generalized-gradient approximation within density functional theory. *J. Chem. Phys.* **109**, 6626–6630 (1998).
26. Ito, M. *et al.* Behaviours and Electronic Structures of Na and Cu Nanoclusters: The Role of *sp-d* Hybridization. *Int. J. Modern Physics B* **19**, 2421–2426 (2005).
27. Hatada, K. *et al.* Full-potential multiple scattering for x-ray spectroscopies. *Phys. Rev. B* **76**, 060102–060106(R) (2007).
28. Hatada, K. *et al.* Full-potential multiple scattering theory with space-filling cells for bound and continuum states. *J. Phys.: Cond. Matt.*, **22**, 185501–185524 (2010).
29. Li, X. *et al.* Experimental Observation and Computation of Icosahedral $W@Au_{12}$ and $Mo@Au_{12}$ Molecules. *Angew Chem. Int. Ed.* **41**, 4786–4789 (2002).
30. Chou, J. P. *et al. Ab initio* random structure search for 13-atom clusters of fcc elements. *J. Phys.: Condens. Matter* **25**, 125305–7 (2013).
31. Ertl, G. *Catalytic Ammonia Synthesis* Jennings, J. R. (ed.) 109–131 (Plenum Press, New York, 1991).
32. Johnson, P. S. *et al.* Universal mechanism for breaking amide bonds by ionizing radiation. *J. Chem. Phys.* **135**, 044702–044709 (2011).
33. Ravel, B. *et al.* Data analysis for X-ray absorption spectroscopy using IFEFFIT. *J. Synchrotron Rad.* **12**, 537–541 (2005).
34. Newville, M. IFEFFIT: interactive XAFS analysis and FEFF Fitting. *ibid*, **8**, 322–324 (2001).
35. Hayakawa, K. *et al.* Progresses in the MXAN Fitting Procedure. *AIP Conf. Proc.* **882**, 111–113 (2007).
36. Lee, C. *et al.* Development of the Colle-Salvetti correlation-energy formula into a function of the electron density. *Phys. Rev. B*, **37**, 785–789 (1988).

37. Hay, P. J. & Wadt, W. R. *Ab initio* effective core potentials for molecular calculations. Potentials for the transition metal atoms Sc to Hg. *J. Chem. Phys.* **82**, 270–285 (1985).
38. Dunning Jr, T. H. & Hay, P. J. *Modern Theoretical Chemistry* Vol. **3** Schaefer III, H. F. (ed.) 1–28 (Plenum, New York, 1976).
39. Yan, M. *et al.* Structure and shape variation in intermediate-size copper clusters. *J. Chem. Phys.* **124**, 024308–6 (2006).

Acknowledgments

The authors would like to thank Y. Niwa for technical assistance during the synchrotron experiments performed under Proposal 2010G097 supported by CREST. The DFT calculations were performed using the computational facilities at the Research Institute for Information Technology, Kyushu University. A part of this work was supported by European FP7 MSNano network under Grant No. PIRSES-GA-2012-317554.

Author contributions

All authors contributed substantially to this work. H.O. and Y.O. wrote the main manuscript text and figures 1–5. The experiments were performed by H.O., Y.O., L.Z., K.Y., H.N., M.U., A.F. and Y.O. while Y.O. carried out the DFT calculation. K. Hay. and K. Hat. performed the FPMS calculations of XANES while Z.S. analyzed the EXAFS experimental data. H.M. coordinated the research team. All authors reviewed the manuscript.

Additional information

Supplementary information accompanies this paper at http://www.nature.com/scientificreports

Competing financial interests: The authors declare no competing financial interests.

How to cite this article: Oyanagi, H. *et al.* Nanoclusters Synthesized by Synchrotron Radiolysis in Concert with Wet Chemistry. *Sci. Rep.* **4**, 7199; DOI:10.1038/srep07199 (2014).